

Self-contained two-layer shallow water theory of strong internal bores

Jānis Priede

Centre for Fluids and Complex Systems,
Coventry University, UK

(Received xx; revised xx; accepted xx)

A theoretical model is proposed for interfacial gravity waves containing strong bores (hydraulic jumps). The model is based on the locally conservative form of shallow-water momentum equation for the two-layer system bounded by a rigid lid. Using a linear combination of the basic irrotationality conservation equations to eliminate the pressure gradient along the interface, we obtain a generalised local momentum conservation equation which contains a free parameter α . This parameter defines the relative contribution of each layer to the pressure at the interface and is supposed to depend on the ratio of densities which is the sole dimensionless parameter in this problem. For nearly equal densities, symmetry considerations suggest $\alpha \approx 0$, which corresponds to both layers affecting the pressure with equal weight coefficients. The front propagation velocities that follow from this assumption and the Rankine-Hugoniot jump conditions for the mass and momentum conservation equations agree well with experimental and numerical results in a wide range of bore strengths. A remarkably better agreement with high-accuracy numerical results for both gravity currents and strong bores is produced by $\alpha = \sqrt{5} - 2$. This is an exceptional point at which the gravity current speed becomes a monotonically increasing function of its depth. With $\alpha = \pm 1$, our model reproduces the classical front conditions due to Wood & Simpson (1984, *J. Fluid Mech.* **140**, 329) and Klemp *et al.* (1997, *J. Fluid Mech.* **331**, 81), which are commonly thought to be outside the scope of the hydrostatic shallow-water approximation. In contrast to previous shallow-water models, our locally conservative momentum conservation equation requires no external closure conditions and provides a unified framework for numerical modelling of strong internal bores and gravity currents.

1. Introduction

Shallow-water approximation is commonly used in the geophysical fluid dynamics to model ocean currents and large-scale atmosphere circulation (Pedlosky 1979). Because such flows are typically dominated by inertia and occur on a horizontal length scale which is much larger than their depth, they can be treated as effectively horizontal and vertically invariant. This simplifies the fluid flow problem from three to two spatial dimensions thus essentially reducing the computational complexity of such flows. Shallow-water approximation can also be used to model long gravity waves on the liquid surfaces or interfaces in stably stratified fluid layers. The latter type of systems are not only routinely used as simplified models of internal waves in oceans (Helfrich & Melville 2006) but are also encountered in the technological applications like aluminium reduction cells Davidson (2001) and the recently developed liquid metal batteries (Kelley & Weier 2018).

Shallow-water waves are generally known to become steeper with time and to develop vertical fronts analogous to the shock waves in the gas dynamics (Courant & Friedrichs 1948). In the fluid dynamics, such shocks are called hydraulic jumps or bores (Stoker

1958) – both terms are used interchangeably here. Hydraulic jumps can also be created by the initial state of fluid, for example, when the flow starts by breaking a dam or when a lock that separates two liquids with different densities is opened (Esler & Pearce 2011).

Mathematically, shock waves correspond to discontinuities in the wave amplitude. It is commonly assumed that although the partial differential equations (PDEs) which govern the wave propagation cease to apply at the discontinuities, the relevant physics, which is represented by the conservation laws behind these equations, may still hold (Whitham 1974). Thus the propagation of shock waves is expected to be governed not by the original PDEs but by equivalent integral relationships which are known as the Rankine-Hugoniot conditions in the gas dynamics. Such relationships can be obtained by integrating the governing PDEs across a discontinuity provided that PDEs are in the form $\partial_t M(\mathbf{v}) + \partial_x N(\mathbf{v}) = 0$. This type of equation represents a local conservation law for the quantity M with the flux N and the dynamical variables $\mathbf{v}(x, t)$.

For single-layer shallow-water flows, there is an infinite number of such local conservation laws (Benney 1973; Miura 1974), whereas only six linearly independent laws exist for the two-layer system with a free surface (Ovsyannikov 1979; Montgomery & Moodie 2001; Barros 2006). For the two-layer system bounded by a rigid lid, which is the focus of this paper, an infinite number of conservation laws is expected (Ovsyannikov 1979; Milewski & Tabak 2015). However, only three most elementary laws expressing the conservation of mass, irrotationality (zero vorticity) and energy are generally known. No local conservation law for momentum appears to be known in this case. On the other hand, the conservation of momentum is of primary importance as it is known to govern the dynamics of hydraulic jumps in single shallow-water layer, which is the limiting case of the two-layer system when the top layer density or the bottom layer depth becomes small (Stoker 1958).

The lack of local momentum conservation law has led to a common belief that the two-layer shallow water equations are inherently non-conservative (Abgrall & Karni 2009) and unable to describe internal hydraulic jumps without additional closure relations. The latter are usually deduced by dimensional arguments (Abbott 1961) or derived using various semi-empirical and approximate integral models (Baines 1995). For gravity currents, which are created when a layer of heavier liquid is driven by its weight along the bottom into a lighter ambient fluid, such a front condition relating the velocity of propagation with the layer depth is the central result of the celebrated Benjamin's theory (Benjamin 1968). This hydraulic-type condition and its various empirical extensions (Klemp *et al.* 1994; Huppert 2006) are commonly regarded indispensable for theoretical description and numerical modelling of gravity currents using shallow-water equations (Ungarish 2011; Rotunno *et al.* 2011).

A number of analogous semi-empirical front conditions have been proposed also for internal bores (Yih & Guha 1955; Baines 1984; Wood & Simpson 1984; Klemp *et al.* 1997). Despite the long history of this problem, there is still no comprehensive theoretical description of internal bores, and new models and front conditions continue to emerge (Borden *et al.* 2012; Borden & Meiburg 2013; Baines 2016; Ungarish & Hogg 2018) due to the importance such bores play in various geophysical flows ranging from the coastal oceans (Scotti & Pineda 2004) to the inversion layers in the atmosphere (Christie & White 1992).

In this paper, we propose a principally new theoretical framework for analysis and numerical modelling of interfacial waves with hydraulic jumps, which in contrast to previous models is completely self-contained and does not require external closure conditions. The theory is based on a locally conservative momentum equation for the two-layer shallow-water system bounded by a rigid lid.

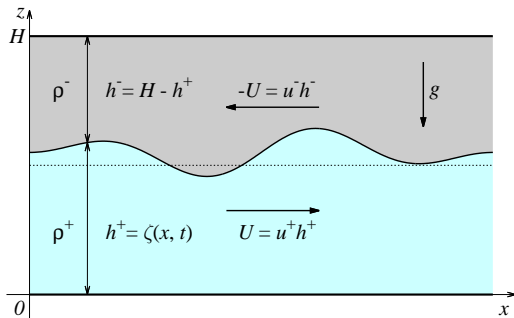


FIGURE 1. Sketch of the problem formulation showing a horizontal channel of constant height H bounded by two parallel solid walls and filled with two inviscid immiscible fluids with constant densities ρ^+ and ρ^- , where $h^+ = \zeta(x, t)$ and $h^- = H - h^+$ are the depths of the bottom and top layers, respectively.

The paper is organized as follows. In the next section, we introduce the two-layer model and derive shallow-water equations in locally conservative form for fluids with arbitrary as well as nearly equal densities. Jump conditions for the latter are derived in section §3, where we also compare the resulting front speeds with the predictions of some previous models as well as with the available experimental and numerical data. The paper is concluded with a summary and discussion of the main results in section §5.

2. Two-layer shallow-water model

Consider a horizontal channel of constant height H bounded by two parallel solid walls and filled with two inviscid immiscible fluids with constant densities ρ^+ and ρ^- as shown in figure 1. The fluids are subject to a downward gravity force with the free fall acceleration g . The interface separating the fluids at the horizontal position x and time instant t is located at the height $z = \zeta(x, t)$, which is equal to the depth of the bottom layer $h^+ = H - h^-$, where h^- is the depth of the top layer. The velocity \mathbf{u}^\pm and pressure p^\pm in both layers is governed by the Euler equation

$$\partial_t \mathbf{u} + \mathbf{u} \cdot \nabla \mathbf{u} = -\rho^{-1} \nabla p + \mathbf{g} \quad (2.1)$$

and the incompressibility constraint $\nabla \cdot \mathbf{u} = 0$. Henceforth, for the sake of brevity, we drop the \pm indices when analogous expressions apply to both layers. At the interface, $z = \zeta(x, t)$, we have the continuity of pressure, $[p] \equiv p^+ - p^- = 0$, and the kinematic condition

$$w = \frac{d\zeta}{dt} = \zeta_t + u\zeta_x, \quad (2.2)$$

where u and w are the x and z components of velocity, and the subscripts t and x stand for the respective partial derivatives. Integrating the incompressibility constraint over the depth of layer and using (2.2), we obtain

$$h_t + (h\bar{u})_x = 0, \quad (2.3)$$

where the overbar denotes the average over the layer depth. Similarly, averaging the horizontal (x) component of (2.1) over the layer depth, we have

$$(h\bar{u})_t + (h\overline{u^2})_x = -\rho^{-1} h\overline{p_x}. \quad (2.4)$$

Pressure is obtained by integrating vertical (z) component of (2.1) as follows

$$p(x, z, t) = \Pi(x, t) + \rho \int_{\zeta}^z (w_t + \mathbf{u} \cdot \nabla w - g) dz, \quad (2.5)$$

where the constant of integration, $\Pi(x, t) = p^{\pm}(x, z, t)|_{z=\zeta}$, defines the pressure distribution along the interface. Averaging the x -component of the gradient of (2.5) over the layer depth, after a few rearrangements, yields

$$\overline{p_x} = \left(\Pi + \rho g \zeta + \rho \overline{(z - z_0)(w_t + \mathbf{u} \cdot \nabla w)} \right)_x, \quad (2.6)$$

which defines the RHS of (2.4) with $z_0 = 0$ and $z_0 = H$ for the bottom and top layers, respectively.

Shallow-water equations follow as an approximation to the exact depth-averaged equations above when the characteristic horizontal length scale of the flow L is assumed to be much larger than the layer depth H : $H/L = \epsilon \ll 1$. Then the incompressibility constraint implies $w/u = O(\epsilon)$ and, respectively, (2.6) reduces to

$$\overline{p_x} = (\Pi + \rho g \zeta)_x + O(\epsilon^2), \quad (2.7)$$

where the leading order term is purely hydrostatic and the $O(\epsilon^2)$ represents a small dynamical pressure correction due to the vertical velocity w .

In addition, the flow is assumed to be irrotational: $\boldsymbol{\omega} = \nabla \times \mathbf{u} = 0$. According to the vorticity equation, $\frac{d\boldsymbol{\omega}}{dt} = \boldsymbol{\omega} \cdot \nabla \mathbf{u}$, this property is preserved by (2.1). In the leading order approximation, $\boldsymbol{\omega} = 0$ reduces to $\partial_z u^{(0)} = 0$, which means that the horizontal velocity can be represented as

$$u = \bar{u} + \tilde{u}, \quad (2.8)$$

where the deviation from average $\tilde{u} = O(\epsilon^2)$ is implied by (2.7). Consequently, $\overline{u^2} = \bar{u}^2 + O(\epsilon^4)$ can be applied to the second term of (2.4). Finally, using (2.3) and ignoring the $O(\epsilon^2)$ dynamic pressure correction, (2.4) can be written as

$$\rho(\bar{u}_t + \frac{1}{2}\bar{u}^2_x + g\zeta_x) = -\Pi_x, \quad (2.9)$$

which together with (2.3) constitute the basic set of shallow-water equations in the leading-order (hydrostatic) approximation.

For completeness, note that the vertical velocity distribution, which is outside the scope of present study, follows directly from the incompressibility constraint and (2.8):

$$w(z) = - \int_{z_0}^z u_x dz = -(z - z_0)\bar{u}_x + O(\epsilon^2), \quad (2.10)$$

where z_0 chosen as in (2.6) to satisfy the impermeability conditions, $w(0) = w(H) = 0$. Then (2.6) leads straightforwardly to the well-known result (Green & Naghdi 1976; Liska *et al.* 1995; Choi & Camassa 1999)

$$\overline{hp_x^{(1)}} = -\frac{1}{3}\rho(h^3(D\bar{u}_x - \bar{u}_x\bar{u}_x))_x + O(\epsilon^4) = \frac{1}{3}\rho(h^2D^2h)_x + O(\epsilon^4),$$

where $D \equiv \partial_t + \bar{u}\partial_x$, and $\bar{u}_x = -h^{-1}Dh$ follows from (2.3) and ensures that (2.2) is satisfied by (2.10) up to $O(\epsilon^2)$.

On one hand, the wave dispersion caused by this weakly non-hydrostatic pressure correction can prevent the development of discontinuities and enable formation of solitary waves and smooth wave fronts (Choi & Camassa 1999). On the other hand, it limits the applicability of this approximation to relatively shallow waves and, thus, excludes

strong internal bores (Esler & Pearce 2011). The latter are the main focus of the present study which shows that such bores can be described by the hydrostatic shallow-water approximation in a self-contained way.

The system of four shallow-water equations (2.9) and (2.3) contains five unknowns, u^\pm , h^\pm and Π , and is closed by adding the fixed height constraint $\{h\} \equiv h^+ + h^- = H$. Henceforth, we simplify the notation by omitting the bar over u and use the curly brackets to denote the sum of the enclosed quantities. Two more unknowns can be eliminated as follows. Firstly, adding the mass conservation equations for both layers together and using $\{h\}_t \equiv 0$, we obtain $\{uh\} = \Phi(t)$, which is the total flow rate. Here we assume the channel to be laterally closed, which means $\Phi \equiv 0$ and, thus, $u^-h^- = -u^+h^+$. Secondly, the pressure gradient Π_x can be eliminated by subtracting the two equations (2.9) one from another. This leaves only two unknowns, $U \equiv u^+h^+$ and $h = h^+$, and two equations, which can be written in locally conservative form as

$$(\{\rho/h\}U)_t + \left(\frac{1}{2}[\rho/h^2]U^2 + g[\rho]h\right)_x = 0, \quad (2.11)$$

$$h_t + U_x = 0, \quad (2.12)$$

where the square brackets are used to denote the difference of the enclosed quantities between the bottom and top layers: $[f] \equiv f^+ - f^-$. In this form, both equations can in principle be integrated across a discontinuity to obtain the corresponding jump conditions. However, this is not the only possible set of locally conservative equations for the two-layer system.

The applicability of (2.11) and (2.12) to strong bores depends on the conservation of the respective quantities not only in simple one-dimensional flows described explicitly by these equations but also in more complex three-dimensional turbulent flows which are usual for strong bores. The conservation of mass described by (2.12) in each layer is supposed to hold if fluids are immiscible, which is assumed in this study but may not always be the case (Milewski & Tabak 2015). On the other hand, the conserved quantity in (2.11) can be represented as $\{\rho/h\}U dx = [\rho u] = \int_H \partial_z(\rho u) dz$. In each layer separately, we have $\partial_z(\rho u) = \rho\omega$, where $\omega = \partial_z u \equiv 0$ is the vorticity in the hydrostatic approximation. It means that (2.11) relies on the conservation of irrotationality (zero vorticity) of flow in each layer. This conservation law is expected to hold as long as the effect of viscosity is negligible which is not necessarily the case in hydraulic jumps where viscous effects may become significant due to sharp velocity gradients and cause energy dissipation even in the zero viscosity limit (Whitham 1974). On the other hand, the conserved quantity in (2.11) is related to the circulation $\oint \rho \mathbf{u} \cdot d\mathbf{r} = \int_\Gamma [\rho u] dx$ around a segment of interface Γ , which represents a vorticity sheet. Consequently, (2.11) is a result of integration of the two-dimensional vorticity-type conservation equation over the depth (Borden & Meiburg 2013). As it is well known from the constant density case, vorticity is conserved only in two-dimensional flows, which advect the vortices, whereas it is not in general the case for three-dimensional flows which can generate vorticity by stretching and twisting of vortices. This again implies that the jump condition resulting from (2.11) may not be applicable to strong bores in two-layer systems as the analogous condition is not applicable in the limiting single-layer case.

The quantity which is conserved across a hydraulic jump in single shallow-water layer with smooth bottom (Kalisch *et al.* 2017) and hence also expected to be conserved in two-layer system with flat top and bottom boundaries is the momentum. In contrast to the circulation and energy, there is no physical mechanism which could disrupt conservation of momentum in a flow of inviscid fluid in such systems.

A momentum conservation law is obtained by first multiplying (2.9) for each layer with

h^\pm and then adding the equations together. Using (2.12) and the fixed height condition, we have

$$[\rho]U_t + (\{\rho/h\}U^2 + \frac{1}{2}g[\rho h^2] + H\Pi)_x = 0. \quad (2.13)$$

In this form, the momentum conservation law is non-local as it contains not only the dynamical variables U and h but also the pressure Π .

The pressure can be eliminated from (2.13) in two alternative ways. First, if we follow the same steps as in deriving (2.13) but before adding the two equations together divide them by ρ^\pm , we obtain

$$\Pi_x = -\{h/\rho\}^{-1} (\{h^{-1}\}U^2 + gHh)_x.$$

Although substituting this expression into (2.13) eliminates Π_x , it does not render the resulting equation locally conservative. The problem is the non-local dependence of the pressure $\Pi = \int \Pi_x dx$ on the U and h . Nevertheless, it is possible to cast (2.13) into a locally conservative form by substituting Π_x in (2.13) directly from (2.9). In this case, however, we are faced with a dilemma as Π_x is defined by two different equations (Ostapenko 1999). Requiring (2.9) for each layer to yield the same Π_x leads to (2.11), which, as discussed above, describes the conservation of circulation.

In general, Π_x can be expressed as a linear combination of (2.9) with the weight coefficients $(1 \pm \alpha)/2$:

$$\Pi_x = -\frac{1}{2} (([\rho/h]U)_t + (\frac{1}{2}\{\rho/h^2\}U^2 + g\{\rho\}h)_x) - \frac{1}{2}\alpha\Lambda, \quad (2.14)$$

where α is an arbitrary constant that defines contribution of each layer to Π_x and Λ equals the LHS of (2.11). Note that with $\alpha = 1$, Π_x is determined only by the top layer, whereas the opposite is the case with $\alpha = -1$. Owing to (2.11) we have $\Lambda = 0$, and hence the last term in (2.14) containing α vanishes. Substituting (2.14) into (2.13), we obtain

$$([\rho - \frac{1}{2}H\rho/h]U)_t + (\{\rho/h - \frac{1}{4}H\rho/h^2\}U^2 + \frac{1}{4}g[\rho]\{h^2\})_x = 0, \quad (2.15)$$

which is the sought locally conservative form of the momentum equation.

Note that (2.15) is equivalent to (2.11) and can be reduced to the latter by using (2.12) provided that U and h are differentiable at least once. For discontinuous solutions, this is no longer the case and therefore (2.11) and (2.15) cannot in general be satisfied simultaneously. In this case, we cannot assume $\Lambda = 0$ and hence the term $-\frac{1}{2}\alpha H\Lambda$ remains in (2.15). As Λ equals the LHS of (2.11), which is locally conservative, this extra term preserves the locally conservative form of the resulting equation. Subsequently, this extended equation, which contains extra term with α , will be referred to as the generalized momentum equation.

Since α is a dimensionless constant, it can depend only the ratio of densities, which is the sole dimensionless parameter in this problem. As Π_x is supposed to vanish when the top layer density ρ^- becomes small and the two-layer system reduces to that of the single layer, (2.9) suggests that Π_x has to be determined solely by the top layer in this limit. As discussed above, this corresponds to $\alpha \rightarrow 1$. In the opposite limit of a small density difference, one could expect $\alpha \rightarrow 0$, which corresponds to both layers affecting Π_x with equal weight coefficients. In the following, the propagation velocities of strong internal bores resulting from the mass and generalized momentum conservation equation with various α values will be considered and compared with available experimental and numerical results.

We shall also need an energy equation which for each layer is obtained by multiplying (2.9) with U and using (2.12):

$$\rho(U^2/h \pm gh^2)_t + ((\rho(U^2/h^2 \pm 2gh) + 2\Pi)U)_x = -2\Pi h_t, \quad (2.16)$$

where the plus and minus signs correspond as before to the bottom and top layers with h and U standing for h^\pm and U^\pm . As seen, the RHS term, which describes energy exchange between the layers, makes (2.16) non-conservative. The RHS term can vanish in the frame of reference, if one exists, in which the flow is stationary. This, however, is not likely to be the case for strong bores in which the flow is usually turbulent. Nevertheless, this is one of the key assumptions underlying the control-volume method which is commonly used to determine the pressure drop across an internal bore by referring to the energy conservation in one of the layers. Besides being stationary the flow in the control volume is assumed to be continuous. These two assumptions are mutually incompatible in the hydrostatic shallow-water approximation in which a solution that is stationary cannot be continuous. As the control-volume method just represents an integral form of shallow-water conservation laws, it is effectively subject to the same constraints as the underlying shallow-water approximation. On the other hand, the energy conservation in separate layers presents just a physical interpretation of (2.9), which yields the same pressure drop across discontinuity but does require the flow to be stationary or continuous. The possible ambiguity of this interpretation and the paradoxical results it may produce when applied to hydraulic jumps will be discussed in the conclusion.

The energy equation takes a locally conservative form independent of the frame of reference when both layers are considered together by taking the sum of (2.16):

$$(\{\rho/h\}U^2 + \frac{1}{4}g[\rho][h^2])_t + (([\rho/h^2])U^2 + g[\rho][h])U_x = 0. \quad (2.17)$$

The local mass, circulation, momentum and energy conservation laws defined respectively by (2.12), (2.15) and (2.17) can straightforwardly be integrated across a discontinuity to obtain jump conditions analogous to the Rankine-Hugoniot relations and the Lax entropy constraint in the gas dynamics. It has to be noted that (2.11), (2.15) and (2.17) are mutually equivalent and can be transformed one into another using (2.12) only if h and U are continuous. It means that the jump conditions resulting from these equations cannot in general be satisfied simultaneously. Since the problem is governed by two equations, only the two corresponding jump conditions can be imposed. The choice of two quantities conserved across a discontinuity is not obvious and depends on the physical arguments. Namely, it depends on the effects which are ignored by the shallow-water approximation but can become relevant in strong bores like, for example, viscous dissipation and three-dimensional vorticity generation, mixing (entrainment). If the shallow-water approximation breaks down in a relatively narrow region, then the complex phenomena taking place in that region can be accounted for by applying the relevant conservation laws and treating this region as a discontinuity (Whitham 1974).

In the following, we assume the density difference to be small. This is not only often the case in reality but also simplifies the problem significantly. Then according to the Boussinesq approximation, the density difference can be neglected for the inertia but not for the gravity of fluids. We slightly extend this approximation by neglecting the deviation of density from its average which is subsequently used as the characteristic value instead of the density of one of the layers. Then (2.15) reduces to

$$([h][u])_t + \frac{1}{4}((H - 3[h]^2/H)[u]^2 + 2g[h]^2[\rho]/\{\rho\})_x = 0, \quad (2.18)$$

where we have assumed $\alpha = 0$ as discussed earlier. The problem is simplified further by using the total height H and the characteristic gravity wave speed $C = \sqrt{2Hg[\rho]/\{\rho\}}$ as the vertical length and velocity scales together with the horizontal length scale L and the time scale L/C . Then (2.18) and (2.17) can be written in the following dimensionless

form

$$(\eta\vartheta)_t + \frac{1}{4}(\eta^2 + \vartheta^2 - 3\eta^2\vartheta^2)_x = 0, \quad (2.19)$$

$$(\eta^2 + \vartheta^2 - \eta^2\vartheta^2)_t + (\eta\vartheta(1 - \eta^2)(1 - \vartheta^2))_x = 0, \quad (2.20)$$

where $\eta = [h]$ and $\vartheta = [u]$ are the dimensionless depth and velocity differentials between the bottom and top layers which emerge as natural variables for this problem. Subsequently, the former is referred to as the interface height and the latter as the shear (or baroclinic) velocity. In the new variables and Boussinesq approximation, (2.11) and (2.12) take a remarkably symmetric form (Milewski & Tabak 2015)

$$\vartheta_t + \frac{1}{2}(\eta(1 - \vartheta^2))_x = 0, \quad (2.21)$$

$$\eta_t + \frac{1}{2}(\vartheta(1 - \eta^2))_x = 0. \quad (2.22)$$

Then the generalized momentum conservation equation, which corresponds to (2.18) with the RHS given by the product of (2.11) and $-\frac{1}{2}\alpha H$, can be written as

$$((\eta + \alpha)\vartheta)_t + \frac{1}{4}(\eta^2 + \vartheta^2 - 3\eta^2\vartheta^2 + 2\alpha\eta(1 - \vartheta^2))_x = 0. \quad (2.23)$$

This equation represents a linear combination of (2.19) and (2.21) in which the latter equation is multiplied with α . Respectively, the basic momentum conservation law (2.19) corresponds to $\alpha = 0$, whereas the circulation conservation law (2.21) to $\alpha \rightarrow \infty$.

Note that owing to the equivalence of various local conservation laws for continuous solutions, (2.19) and (2.20) can be derived directly from (2.21) and (2.22), and an infinite sequence of conservation laws can be constructed starting from the basic quasi-linear form of equations (Milewski & Tabak 2015). Equations (2.21) and (2.22) can also be written in the canonical form

$$R_t^\pm - \lambda^\pm R_x^\pm = 0, \quad (2.24)$$

where $R^\pm = -\eta\vartheta \pm ((1 - \eta^2)(1 - \vartheta^2))^{1/2}$ are the Riemann invariants and

$$\lambda^\pm = \frac{3}{4}R^\pm + \frac{1}{4}R^\mp \quad (2.25)$$

are the associated characteristic velocities (Long 1956; Cavanie 1969; Ovsyannikov 1979; Sandstrom & Quon 1993; Baines 1995). For interface confined between the top and bottom boundaries, which corresponds to $\eta^2 \leq 1$, the characteristic velocities are real and, respectively, the equations are of hyperbolic type if $\vartheta^2 \leq 1$. The latter constraint on the shear velocity is required for the stability of interface, which otherwise would be disrupted by the long-wave shear instability (Milewski *et al.* 2004).

3. Jump conditions

Consider a discontinuity in η and ϑ at the point $x = \xi(t)$ across which the respective variables jump by $[\eta] \equiv \eta_+ - \eta_-$ and $[\vartheta] \equiv \vartheta_+ - \vartheta_-$. Here, the plus and minus subscripts denote the respective quantities in the front and back of the jump; the double-square brackets stand for the differential of the enclosed quantity across the jump. Integrating (2.22) and (2.23) across the jump, which is equivalent to substituting the spatial derivative f_x with $[[f]]$ and the time derivative f_t with $-\dot{\xi}[[f]]$ (Whitham 1974), the jump propagation velocity can be expressed as

$$\dot{\xi} = \frac{1}{2} \frac{[[\vartheta(1 - \eta^2)]]}{[[\eta]]} = \frac{1}{4} \frac{[[\eta^2 + \vartheta^2 - 3\eta^2\vartheta^2 + 2\alpha\eta(1 - \vartheta^2)]]}{[[(\alpha + \eta)\vartheta]]}. \quad (3.1)$$

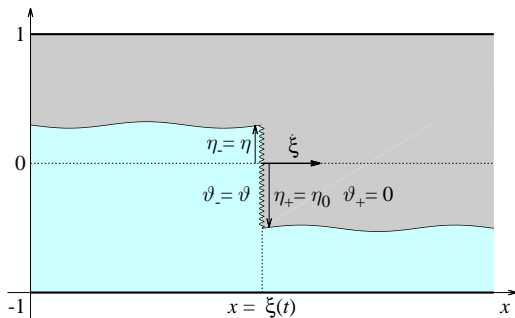


FIGURE 2. A jump with the upstream interface height $\eta_- = \eta$ and shear velocity $\vartheta_- = \vartheta$ propagating at velocity $\dot{\xi}$ into a still fluid ahead ($\vartheta_+ = 0$) with the interface located at the height $\eta_+ = \eta_0$.

As for the single layer, jump conditions above consist of two equations and contain five unknowns, η_{\pm} , ϑ_{\pm} and $\dot{\xi}$. It means that two unknown parameters can be determined when the other three are known. The non-linearity of jump conditions (3.1) implies a possibility of multiple solutions, some of which may be unphysical. Additional constraint on the feasible hydraulic jumps follows from (2.20) and the associated energy variation:

$$\left[\eta \vartheta (1 - \eta^2)(1 - \vartheta^2) - \dot{\xi} (\eta^2 + \vartheta^2 - \eta^2 \vartheta^2) \right] = \dot{\varepsilon} \leq 0, \quad (3.2)$$

which cannot be positive as the mechanical energy can only be dissipated or carried away by dispersive waves (Ali & Kalisch 2010) but not generated by fluid flow.

Next, let us apply the general jump conditions derived above to a bore with the interface height $\eta_- = \eta$ which propagates with an unknown shear velocity $\vartheta_- = \vartheta$ into a still fluid ahead ($\vartheta_+ = 0$) with the interface located at the height $\eta_+ = \eta_0$ as shown in figure 2. After a few rearrangements (3.1) yields

$$\vartheta^{\pm} = \pm \frac{(\eta_0 - \eta)(\eta_0 + \eta + 2\alpha)^{1/2}}{((1 - \eta^2)(\eta_0 - \eta) + 2(\eta + \alpha)(1 - \eta_0\eta))^{1/2}}, \quad (3.3)$$

$$\dot{\xi}^{\pm} = -\vartheta^{\pm} \frac{1 - \eta^2}{2(\eta_0 - \eta)}, \quad (3.4)$$

where the plus and minus signs refer to the opposite directions of propagation, $\dot{\xi}^+ = -\dot{\xi}^-$, which are admitted by the mass and momentum conservation for a bore of given height. Note that the propagation velocity of weak bores ($\eta \rightarrow \eta_0$) reduces to the respective characteristic velocity (2.25): $\dot{\xi}^{\pm} \rightarrow \lambda^{\pm}$, which defines the speed of small-amplitude disturbances. Because the energy flux (3.2) changes sign with the direction of propagation, only one direction of propagation is admitted for a bore of given height with quiescent fluid on one side. The front (η_0) and back (η) heights of bores admitted by the hyperbolicity constraint, $0 \leq \vartheta^2 \leq 1$, and the respective direction of propagation are shown in figure 3 for various α . As noted above, with $\alpha = 0$ and $\alpha = \infty$, the generalised momentum equation reduces to (2.19) and (2.21), whereas $\alpha = 1$ and $\alpha = -1$ describe a pressure drop across discontinuity determined solely by the top and bottom layers, respectively. The front and back heights for which the hyperbolicity constraint is satisfied depend on α . For each combination of heights, a bore propagating either downstream ($\dot{\xi} > 0$) or upstream ($\dot{\xi} < 0$) is in principle possible depending on the energy dissipation

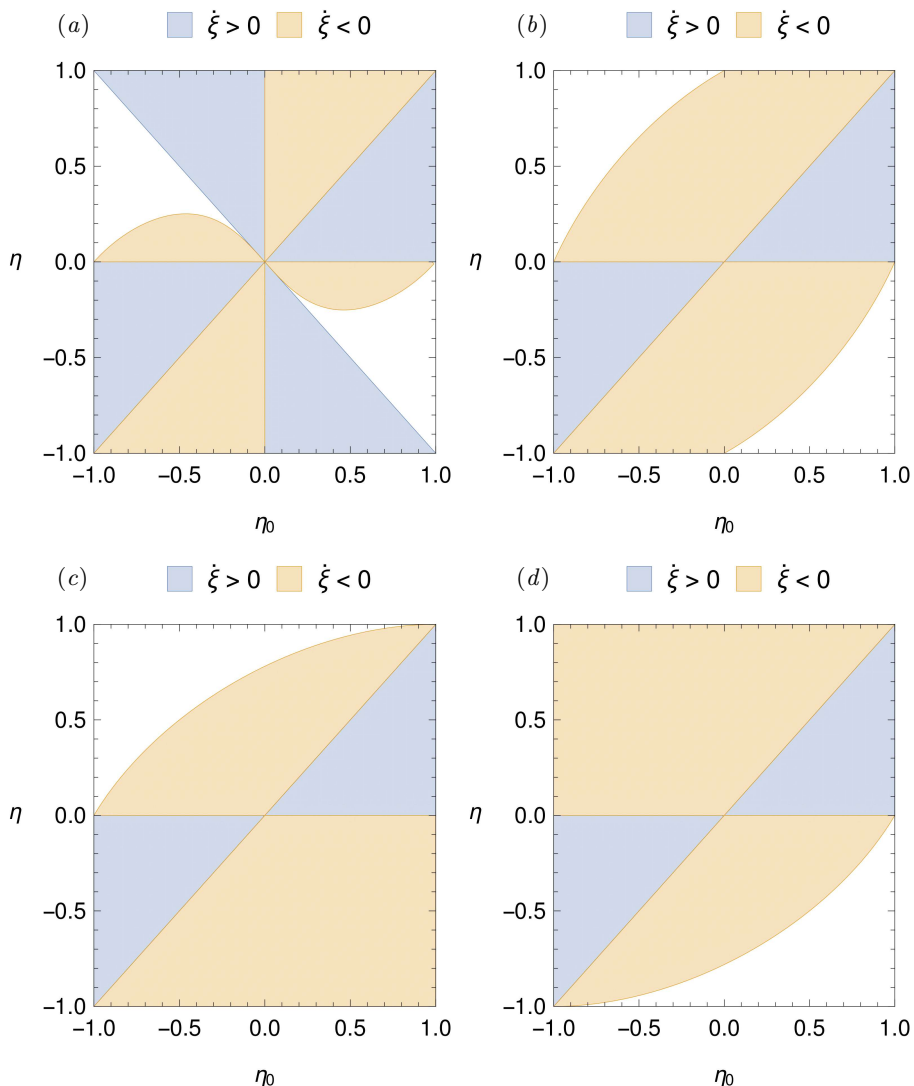


FIGURE 3. The front (η_0) and back (η) heights of internal bores permitted by the hyperbolicity constraint $0 \leq \vartheta^2 \leq 1$ for $\alpha = 0$ (a), ∞ (b), -1 (c), 1 (d). The downstream ($\dot{\xi} > 0$) and upstream ($\dot{\xi} < 0$) directions of propagation are defined by the energy dissipation constraint $\dot{\epsilon} \leq 0$.

constraint. The respective regions for $\alpha = 0$ and $\alpha = \infty$ are centrally symmetric, whereas for $\alpha = \pm 1$ they are centrally reflected images of each other. As seen, the last two values exclude bores with $\eta_0 \rightarrow \pm 1$ which correspond to deep and shallow quiescent states on the right of the front.

Gravity currents, which propagate along the bottom $\eta_0 = -1$, belong to the latter type. As seen in figure 3, the gravity current depth is limited to the lower half of channel ($\eta \leq 0$) by all α except $\alpha = 1$. For a gravity current propagating downstream, (3.3) and

(3.4) yield

$$\vartheta = \left(\frac{(1 + \eta)(1 - \eta - 2\alpha)}{1 - \eta^2 - 2(\alpha + \eta)} \right)^{1/2}, \quad (3.5)$$

$$\dot{\xi} = \frac{1}{2}(1 - \eta)\vartheta. \quad (3.6)$$

The front velocity can be written in terms of the traditional front height $h = (1 + \eta)/2$ as

$$\dot{\xi} = (1 - h)\sqrt{\frac{2h(1 - \alpha - h)}{1 - \alpha - 2h^2}}. \quad (3.7)$$

As seen in figure 4, with $\alpha = 0$ this shallow-water (SW) front velocity is generally slightly lower than that resulting from the well-known Benjamin's formula $\dot{\xi} = \sqrt{\frac{h(1-h)(2-h)}{1+h}}$ (Benjamin 1968). On the other hand, the recent vortex-sheet model of Borden & Meiburg (2013) yields a somewhat higher front velocity $\dot{\xi} = (1 - h)\sqrt{2h}$. It is noteworthy that the same condition follows also from the shallow-water circulation conservation equation (2.21) which formally corresponds to $|\alpha| \rightarrow \infty$ in (3.7). Surprisingly, it turns out that that also Benjamin's formula follows from (3.7) with $\alpha = -1$. This corresponds to the pressure along the interface determined solely by the bottom layer.

We include in figure 4 also the recent results of Ungarish & Hogg (2018) for the gravity current speeds obtained by using control-volume method and vortex-wake model in which a mixing layer is assumed instead of the usual sharp interface. The latter assumption takes this model outside the shallow-water approximation. All models yield the same velocity for thin layers ($h \rightarrow 0$): $\dot{\xi}/\sqrt{h} \rightarrow \sqrt{2}$, where they reproduce the classical result due to von Kármán (Huppert 2006), as well as for the gravity currents that span the lower half of channel ($h = 1/2$): $\dot{\xi}/\sqrt{h} = 1/\sqrt{2}$. For intermediate heights, the SW model (3.7) with $\alpha = 0$ produces in general lower front velocity than the previous models.

Based on the experimental results, it has been suggested by Rottman & Simpson (1983) and Marino *et al.* (2005) that for shallow gravity currents, the normalized front velocity, $\dot{\xi}/\sqrt{h}$, may be closer to 1 rather than $\sqrt{2}$. Numerical results indicate that this discrepancy may be due to turbulent interfacial drag (Klemp *et al.* 1994) or viscosity (Härtel *et al.* 2000). The latter can have a significant effect even on relatively deep gravity currents up to the Reynolds numbers of $O(10^4)$ which are typical for laboratory experiments.

Alternatively, it may be due to the uncertainty in the depth of turbulent gravity currents. As shown at the end of this section, gravity current can be connected upstream to another uniform state of a larger depth. This may lead to a lower-than-expected front velocity when the upstream depth is taken for the front height.

Klemp *et al.* (1994) argue that the height of gravity current may be limited by the characteristic wave velocity (2.25),

$$\lambda^+ = -\eta\vartheta + \frac{1}{2}\sqrt{(1 - \eta^2)(1 - \vartheta^2)},$$

which at a certain critical value becomes lower than the front speed. As seen in figure 5, this is the case for the dimensionless front height $h = (1 + \eta)/2$ larger than

$$h_c = \begin{cases} (\sqrt{3} - 1)/2, & \alpha = 0, \\ 2 \sin(\pi/18), & \alpha = -1, \\ 1/3, & \alpha \rightarrow \infty. \end{cases} \quad (3.8)$$

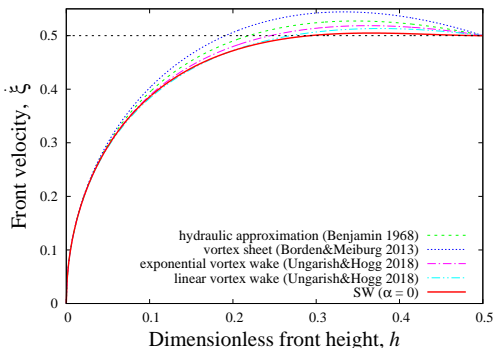


FIGURE 4. The front velocity of gravity current ξ versus the dimensionless front height $h = \frac{1}{2}(1 + \eta)$: comparison of the two-layer shallow-water (SW) model (3.7) with $\alpha = 0$ with the classical hydraulic approximation due to Benjamin (1968), the vortex sheet model of Borden & Meiburg (2013) and the vortex-wake model of Ungarish & Hogg (2018).

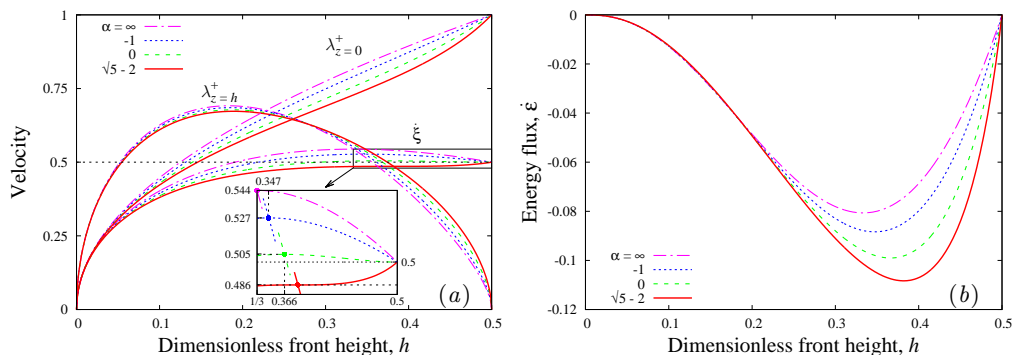


FIGURE 5. The characteristic downstream wave speed λ^+ at the top ($z = h$) and bottom ($z = 0$) of the front and the front velocity ξ versus its height for $\alpha = \infty, -1, 0, \sqrt{5} - 2$ (a) and the respective energy dissipation (b).

As discussed before, the last two values lead to the front conditions of Benjamin (1968) and Borden & Meiburg (2013). However, it is important to notice that a front moving faster than disturbances behind it does not violate the causality, as it is often argued, because at the same shear velocity ϑ , there are faster moving disturbances at the bottom of front ($\eta = -1$).

There are two more noteworthy coincidences that happen at the same critical point. First, as seen in the inset of figure 5, the point at which the characteristic velocity $\lambda_+|_{z=h}$ drops below the respective front speed ξ for each α coincides with the maximum of ξ . The presence of such a maximum implies that gravity currents with $h > h_c$ may be unstable (Benjamin 1968; Baines 2016). Namely, $\frac{d\xi}{dh} < 0$ for $h \geq h_c$ means that a virtual perturbation decreasing the front height h would increase the front speed ξ . Then the mass conservation would enhance the initial perturbation and thus cause the gravity current collapse to a lower depth if one is admitted by the conservation of mass and momentum. This scenario is analyzed in the next section where we consider the possible upstream states to which gravity currents can be connected via a trailing bore.

The second coincidence pointed out already by Benjamin (1968) concerns the energy dissipation rate which also happens to have maximum at exactly the same critical height.

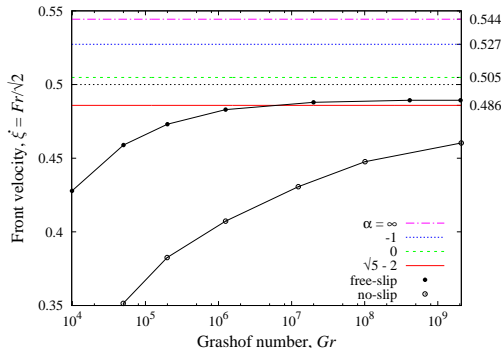


FIGURE 6. Comparison of critical gravity current speeds for various α with the numerical results of Härtel *et al.* (2000) for gravity currents generated by the lock exchange with free-slip and no-slip boundary conditions. The conversion factor of $1/\sqrt{2}$ is due to the channel half-height used as the length scale in the definition of Froude number, Fr , by Härtel *et al.* (2000).

The underlying mechanism and consequences these two rather non-obvious coincidences will be elucidated in the next section.

It is important to note that maximum of front propagation velocity coincides with the characteristic wave speed for the respective gravity current depth only for

$$\alpha < \alpha_c = \sqrt{5} - 2 \approx 0.236. \quad (3.9)$$

The same applies to the coincidence of maximal dissipation rate and the propagation velocity. For $\alpha > \alpha_c$, the intersection point of the propagation and characteristic velocities switches over to the local minimum of $\dot{\xi}$, which originally emerges at $\eta = -\alpha < 0$ and moves towards the maximum as α raises above zero. At $\alpha = \alpha_c$, both turning points of $\dot{\xi}$ annihilate each other by merging into a stationary inflection point that is defined by $\partial_\eta^2 \dot{\xi} \Big|_{\eta=-\alpha_c} = 0$, where $h_c = (1 - \alpha_c)/2 \approx 0.382$ and $\dot{\xi} = \alpha_c^{1/2} \approx 0.486$ (see figure 5). A further increase of α causes both turning points of $\dot{\xi}$ reemerge after which local minimum of $\dot{\xi}$ moves back to $h = \frac{1}{2}$ at $\alpha = \frac{1}{2}$. At this point, the maximum of energy dissipation rate switches from the local maximum to minimum of $\dot{\xi}$.

Thus, α_c represents an exceptional point at which the gravity current speed becomes a monotonically increasing function of its depth. It is interesting to note that the gravity current velocity at this point agrees surprisingly well with the highly-accurate numerical results of Härtel *et al.* (2000) for the gravity currents generated by the lock exchange with free-slip boundary conditions (see figure 6). With real no-slip boundary conditions, a much higher Reynolds number seems to be required to achieve this inviscid limit. As shown below, α_c produces a remarkably good agreement with numerical results not only for gravity currents but also for strong bores in Boussinesq fluids.

Now, let us turn to internal bores and compare the propagation velocities following from our shallow-water theory with the predictions of some previous models as well as with the available experimental and numerical results. We limit our comparison to the semi-empirical model of Klemp, Rotunno and Skamarock (KRS) (Klemp *et al.* 1997), the vortex-sheet model of Borden and Meiburg (BM) (Borden & Meiburg 2013) and the vortex-wake model of Ungarish and Hogg (UH) (Ungarish & Hogg 2018). For better agreement with experimental results, it is assumed in the KRS model that energy is dissipated only in the top layer, which shrinks as the bore advances. On the other hand, the BM model has been derived using the vorticity equation for bores in the Boussinesq

fluids. However, as noted above, vorticity may not be conserved in turbulent bores. As for the gravity currents, the BM model yields the same front speed as the shallow-water circulation conservation law (2.21): $\xi = \frac{1}{2}(1 - \eta^2)/(1 - \eta_0\eta)^{1/2}$. In the UH model, the conservation of both circulation and momentum is effectively imposed in addition to that of the mass. This is not possible using only the height averaged quantities in each layer, as in the shallow-water approximation, and requires a non-uniform vertical velocity distribution. The latter is introduced by replacing the sharp interface with a single-parameter mixing layer whose analytical form is not uniquely defined but still affects the results as it may be seen in figure 4.

The aforementioned models are compared in figure 7 with the experimental results of Wood & Simpson (1984), Rottman & Simpson (1983) and Baines (1984) as well as with the two-dimensional numerical results of Borden *et al.* (2012). Note that the density ratio $s = \rho^-/\rho^+ = 0.79$ in (Baines 1984) is somewhat lower than $s = 1$ assumed in the Boussinesq approximation. Nevertheless, no significant deviation of experimental results from the Boussinesq approximation is noticeable when the average density is used as the characterise value. For consistency with previous publications, all front velocities are rescaled with $\sqrt{h_0}$, which is the dimensionless velocity of small-amplitude long interfacial waves when the depth of the bottom layer ahead of the bore is small ($h_0 \ll 1$). The front velocities normalized in this way are plotted in figure 7 against the bore strength h/h_0 , where h is the interface height of the bore. With this normalization, we have $\xi/\sqrt{h_0} \rightarrow 1$ when the layer ahead is thin ($h_0 \rightarrow 0$) and the bore is weak ($h/h_0 \rightarrow 1$). All models can be seen to converge to this basic linear limit. Although the predicted front velocities start to diverge at larger bore strengths, the divergence remains relatively small in comparison to the scatter in the experimental data. All front velocities converge again, similarly to the gravity current velocity in figure 4, when the interface height approaches the mid-plane $h = 0.5$. The SW front velocity (3.4) with $\alpha = 0$ is seen to approach this limit almost monotonously which is due to its distinctive feature, $\frac{d\xi}{dh} = 0$ at $h = 0.5$, whereas all other models produce $\frac{d\xi}{dh} < 0$ at this point. Numerical results for $h_0 = 0.2$ can be seen to reproduce this nearly monotonous variation predicted by the SW model with $\alpha = 0$, though at slightly lower propagation velocities. This difference, which is usually attributed to the turbulent mixing between the layers, may also be due to the viscous loss of momentum at the rigid top and bottom boundaries. Viscous effects are assumed to be negligible in the SW model but could be significant at the relatively small Reynolds number $Re = 3500$ used in the numerical simulation. A remarkably better agreement with numerical results for relatively strong bores is achieved by the SW model with $\alpha = \alpha_c$ (3.9). However, there is no obvious explanation for this good agreement which may be just accidental but still noteworthy.

4. Bores with gravity currents as front states

Now, let us return to the gravity currents and consider possible upstream states which they can be connected to. Instead of the quiescent fluid layer shown in figure 2, the front state is assumed to be a gravity current with the interface height η_0 and the shear velocity $\vartheta_+ = \vartheta_0(\eta)$ defined by (3.5). As before, upstream state with unknown interface height $\eta_- = \eta_1$ and shear velocity $\vartheta_- = \vartheta_1$ needs to be found by solving (3.1). This can be done analytically using the computer algebra software Mathematica (Wolfram 2003), which yields for $\alpha = 0$

$$\vartheta_1^\pm(\eta_1, \eta) = \frac{(\eta_1 + \eta)(1 - \eta_1\eta)\vartheta \pm (\eta_1 - \eta)\gamma}{\eta_1 + \eta - 3\eta_1^2\eta + \eta_1^3}, \quad (4.1)$$

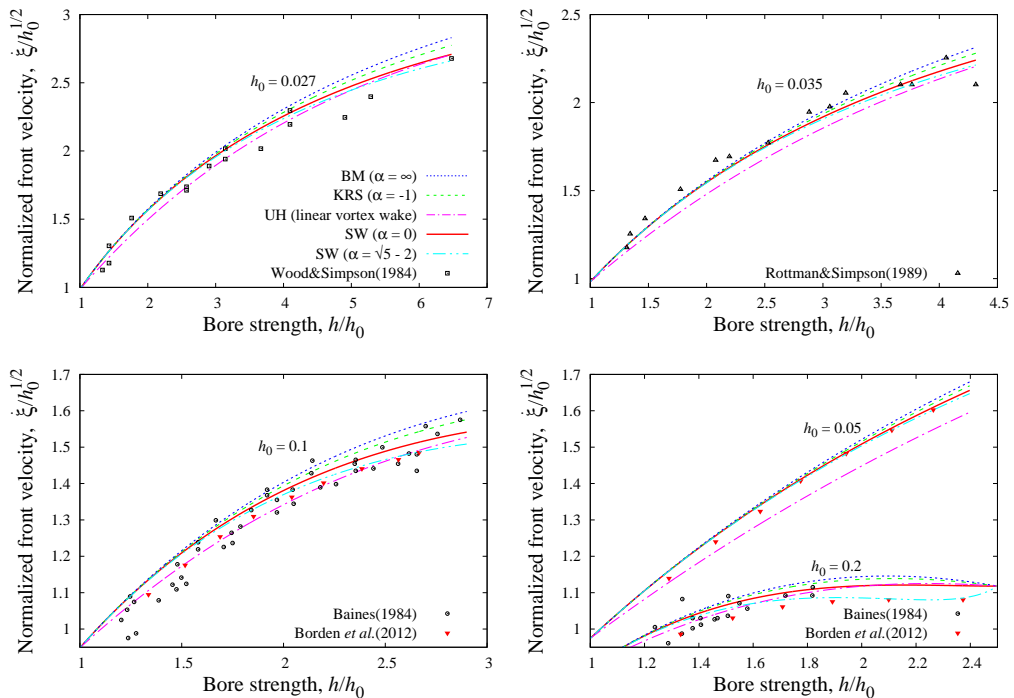


FIGURE 7. The front velocity $\dot{\xi}/\sqrt{h_0}$ normalized with the dimensionless depth of the bottom layer h_0 ahead the bore versus the bore strength h/h_0 for $h_0 = 0.027, 0.035, 0.05, 0.1, 0.2$: comparison of the shallow-water theory (SW, $\alpha = 0, \sqrt{5} - 2$) with KRS (Klemp *et al.* 1997), BM (Borden & Meiburg 2013), UH (Ungarish & Hogg 2018) models as well as with the experimental results of Wood & Simpson (1984), Rottman & Simpson (1983), Baines (1984) and the numerical results of Borden *et al.* (2012).

where $\gamma^2 = \eta^2 ((4\eta_1^2 - 1)\vartheta^2 - 3\eta_1^2 + 1) - 2\eta\eta_1(\eta_0^2 + \vartheta^2 - 1) + \eta_1^2(\eta_1^2 - \vartheta^2 + 1)$ and the plus and minus signs describe two possible branches of the solution. For $\eta_1 = \eta$, which corresponds to a uniform gravity current, (4.1) reduces to $\vartheta_1^\pm = \vartheta$. A similar but somewhat longer solution can be obtained also for general α .

Let us start with a shallow gravity current of depth $h = (1 + \eta)/2 \rightarrow 0$ and assume the upstream depth to be comparably small: $h_1 = (1 + \eta_1)/2 = \kappa h$, where $\kappa = h_1/h = O(1)$. In this limit, the jump velocity (3.1) for (4.1) becomes independent of α :

$$\dot{\xi}_1 = \left(1 \mp \frac{\kappa}{\sqrt{\kappa+1}}\right) \dot{\xi}, \quad (4.2)$$

where $\dot{\xi} = \sqrt{2h}$ is the gravity current velocity for $h \rightarrow 0$. As seen, only the jump velocity defined by the minus sign in (4.2) is lower than $\dot{\xi}$. Consequently, only this solution is feasible. Note that the respective jump velocity drops with the increase of the relative jump height and turns zero at $\kappa_0 = (1 + \sqrt{5})/2$, where the jump becomes stationary. On the other hand, according to the energy balance (3.2), which reduces to

$$\dot{\epsilon} = \frac{4\sqrt{2}(\kappa - 1)^3 (\kappa - \sqrt{\kappa + 1})}{(\kappa + 1)^{3/2}} h^{5/2},$$

this jump is physically feasible with $\dot{\epsilon} \leq 0$ only for $1 \leq \kappa \leq \kappa_0$. It means that shallow gravity currents can be connected to upstream states with the interface height up to a

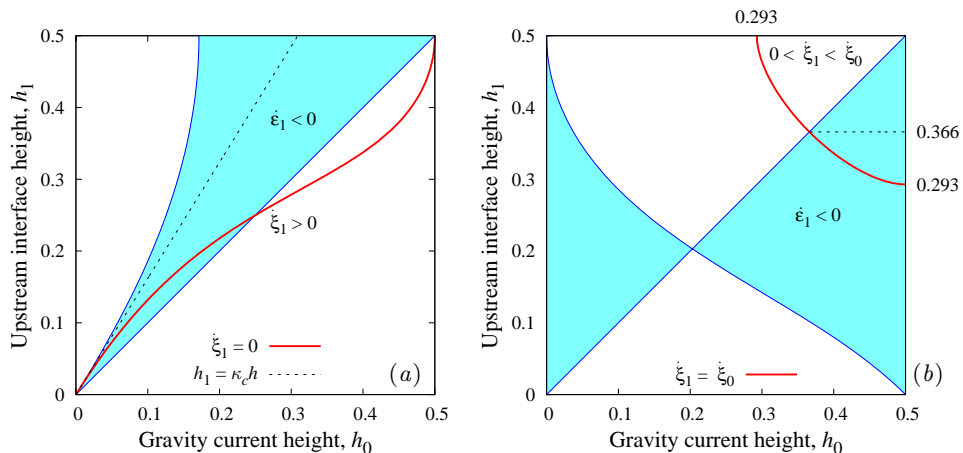


FIGURE 8. The upstream interface height permitted by the energy dissipation constraint $\dot{\epsilon}_1 \leq 0$ versus the gravity current front height for the v_1^+ (a) and v_1^- (b) branches of (4.1) for $\alpha = 0$. The dotted line shows the upper limit for shallow gravity currents and the solid lines show the interface height at which the upstream jump becomes stationary ($\dot{\xi}_1 = 0$) (a) and co-moving ($\dot{\xi}_1 = \dot{\xi}_0$) with the gravity current (b).

factor of $\kappa_0 \approx 1.62$ greater than the gravity current front height. Taking the upstream interface height for the gravity front height can reduce the normalized front speed down to $\dot{\xi}/\sqrt{h_1} = 2/\sqrt{1+\sqrt{5}} \approx 1.11$, which is not far from the empirical value of 1.19 found for $h < 0.075$ by Huppert & Simpson (1980). The exact solution of (3.2) plotted in figure 8 shows that the possible upstream depth for deeper gravity currents is larger than that predicted by the linear relationship. Note that the energy dissipation vanishes at $h_1 = h_0$ and changes sign across this line which describes a uniform gravity current.

First, let us consider the possibility of a shallower gravity current forming at the front of a supercritical current with $h \geq h_c$. This corresponds to a relatively deep leading gravity current connected to a higher upstream state by a single bore that moves in the same direction as the gravity current. As seen in figure 8(a), bores described by the positive branch of (4.1) can move downstream only if the leading gravity current is sufficiently shallow. Bores that can move in the same direction as deep gravity currents are described by the negative branch of (4.1). The respective gravity current and bore heights admitted by the energy dissipation constraint are shown by the filled-in region on figure 8(b). The solid line delimits the range of bores that can move not faster than the leading gravity current. The interface heights that satisfy both constraints are located in the upper right corner below the diagonal line where $h_1 \leq h_0$ on figure 8(b). This corresponds to an upstream state that is shallower than the leading gravity current. The latter, in turn, has to be deeper than the minimal depth defined by the intersection of the diagonal with the solid line along which $\dot{\xi}_1 = \dot{\xi}_0$. This point coincides with the critical depth h_c at which the leading front speed attains maximum. As argued above, the gravity currents deeper than h_c may be unstable.

On the other hand, as it may be seen in figure 8(b), stable gravity currents, which are located in the region above the diagonal with $h_0 < h_c < h_1$, give rise only to energy-generating bores which are unphysical when considered as separate entities. However, such bores can exist together with the leading gravity current front if the total energy is dissipated in the coupled system formed by both jumps. For such a coupled system to

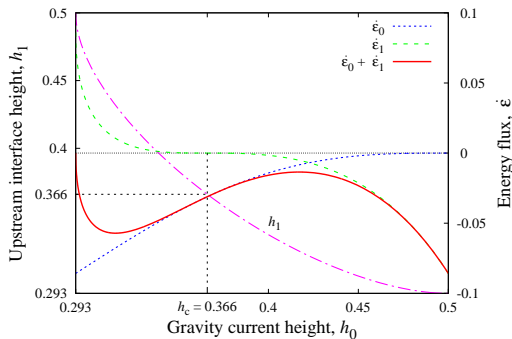


FIGURE 9. The bore height h_1 versus the leading gravity current depth h_0 at which both move at the same speed $\dot{\xi}_1 = \dot{\xi}_0$ and the energy balance for the gravity current ($\dot{\epsilon}_0$) and bore ($\dot{\epsilon}_1$).

form, first of all, the bore has to move at the same velocity as the leading front: $\dot{\xi}_1 = \dot{\xi}_0$. The jump heights that satisfy this constraint are shown by the solid line in 8(b). As seen in figure 9, although the trailing bore generates energy if $h_0 < h_c$, more energy is dissipated by the leading front as long as the upstream state is shallower than the channel mid-height $h_1 = 0.5$. This critical upstream depth produces a leading gravity current of the lowest possible depth $h_0 = 1 - 1/\sqrt{2} \approx 0.293$ for $\alpha = 0$. The respective depths for $\alpha = -1, \infty$ are $(5 - \sqrt{17})/4 \approx 0.219$ and $(3 - \sqrt{5})/4 \approx 0.191$. The decrease of the upstream depth causes the leading gravity current depth rise until both depths become equal at h_c (3.8). At this point, the bore height becomes small and, thus, its velocity of propagation approaches that of small-amplitude disturbances which is defined by the characteristic wave speed λ_+ . This explains why λ_+ coincides with the maximum of $\dot{\xi}$ exactly rather than just approximately as speculated by Baines (2016). It also reveals the duality of the propagation velocity for gravity currents of supercritical depth $h_1 \geq h_c$. Namely, $\dot{\xi} = \dot{\xi}(h_1)$ defines not only the velocity of gravity current of the respective depth but also that of a bore of the same upstream height which trails the gravity current of a subcritical depth $h_0 < h_c$ propagating at the same speed $\dot{\xi} = \dot{\xi}(h_0)$.

5. Summary and discussion

We derived a locally conservative shallow-water momentum equation for the two-layer system bounded by a rigid lid. In contrast to previous theories, no external closure relations are required in our model to describe strong internal bores and gravity currents. So far such closure relations were commonly assumed to be indispensable for the two-layer shallow-water equations and outside the underlying hydrostatic approximation. A momentum equation for two-layer system was obtained in a generalised locally conservative form by using linear combination of the basic shallow-water equations, which describe the conservation of irrotationality in each layer, to eliminate the pressure gradient. As a result of the non-uniqueness of the linear combination used, the momentum conservation equation contains a free dimensionless parameter α which defines the relative contribution of each layer to the pressure at the interface and is supposed to depend on the density ratio. The appearance of α is related with the external length scale, the total height H , in the two-layer system. The existence of H allows us to multiply the circulation conservation equation, which is a lower order conservation law, with αH and add it to the momentum conservation equation, which has the same physical units. This leads to a generalised momentum conservation equation containing α . This parameter is irrelevant

if the circulation and momentum conservation equations are mutually equivalent which is the case only for continuous solutions.

Using symmetry considerations, we argued that the fluid flows with nearly equal densities could be expected to affect the pressure at the interface with the same weight coefficients which corresponds to $\alpha = 0$. The front propagation velocities resulting from this assumption and the Rankine-Hugoniot jump conditions for the mass and momentum equations were compared with the predictions of a number of previous models as well as with numerical and experimental results. A good agreement was found with the existing experimental and numerical results including slightly non-Boussinesq cases. The propagation velocities resulting from the local momentum conservation law appear generally closer to numerical results than the those predicted by the previous models. A remarkably better agreement with high-accuracy numerical results for both gravity currents and strong bores is produced by $\alpha = \alpha_c = \sqrt{5} - 2$, where α_c is an exceptional value at which the gravity current speed becomes a monotonically increasing function of its depth. Currently, there is no definite explanation for this good agreement.

It was also found that the classical front condition for gravity currents due to Benjamin (1968) as well as that its generalisation to internal bores by Klemp, Rotunno and Skamarock (KRS) (1997) are reproduced by our momentum conservation equation with $\alpha = -1$, which corresponds to the pressure at the interface determined entirely by the bottom layer. Similarly, the alternative front condition proposed for internal bores earlier by Wood & Simpson (1984), which is known to break down for shallow gravity currents and does not agree with experimental results as well as the KRS model, is reproduced by our model with $\alpha = 1$. This value describes the pressure at the interface determined entirely by the top layer. In the WS and KRS models, this is interpreted as energy conservation in the top and bottom layers, respectively. Li & Cummins (1998) argue that in general energy can be dissipated in both layers with the WS and KRS models representing two limiting cases and yielding, respectively, the upper and lower limit of the bore velocity. Firstly, it has to be noted that the bore velocities resulting from our model with $\alpha = 0$ are lower than those predicted not only by the WS but also by the KRS model. Secondly, the interpretation in terms of energy conservation in each layer separately is ambiguous in the shallow-water approximation where the energy balance is defined only for the whole two-layer system. Shallow-water equations neither allow nor require to attribute energy dissipation to a specific layer across a hydraulic jump. In the shallow-water approach, the pressure drop across a hydraulic jump in each layer is defined by the basic irrotationality conservation equation. Formally, the same pressure drop can be obtained also from the energy conservation equation for a separate layer by assuming the existence of a co-moving frame of reference in which the solution is stationary. In this case, the energy conservation equation reduces to the Bernoulli equation as does the irrotationality conservation equation.

On one hand, the energy equation for a separate layer is mathematically redundant and provides just a physical interpretation for the pressure drop. On the other hand, it leads to a paradox when applied to interpret the front condition resulting from the shallow-water circulation conservation law. In this case, the pressure drop across discontinuity in each layer is effectively defined by the irrotationality conservation. In the co-moving frame of reference, the latter is equivalent to the energy conservation in the respective layer. Equating pressure drops across discontinuity in both layers enforces the conservation of circulation. The paradox is that the conservation of energy in each layer separately is not equivalent to the conservation of energy in the whole two-layer system. It is due to the fact that the energy for discontinuous solutions cannot in general be conserved simultaneously with the mass and circulation. In addition, solutions which are stationary

in the co-moving frame of reference cannot be continuous in the hydrostatic shallow-water approximation which is effectively used also in the control-volume method. This implies that the energy conservation in separate layers may be inapplicable to hydraulic jumps because it is not compatible with the total energy balance in the two-layer system.

Another serious problem with the circulation is the fact that, in the hydrostatic shallow-water approximation, it cannot be conserved simultaneously with the momentum and mass across a hydraulic jump. There are physical mechanisms, like viscosity and turbulence, which can account for the dissipation of energy and generation of circulation in strong bores. But there are no analogous physical mechanisms that could disrupt momentum balance. Therefore, the momentum conservation, notwithstanding its inherent ambiguity, appears to be more physically relevant than the conservation of circulation.

In conclusion, the locally conservative momentum equation obtained in this study provides a unified theoretical framework for modelling strong internal bores and gravity currents using shallow-water equations for the two-layer system bounded by a rigid lid.

Acknowledgements

I would like to thank M. Ungarish and P. Milewski for bringing their recent papers to my attention as well as for the interesting and stimulating comments.

REFERENCES

- ABBOTT, M. B. 1961 On the spreading of one fluid over another. *La Houille Blanche* **6**, 827–856.
- ABGRALL, R. & KARNI, S. 2009 Two-layer shallow water system: a relaxation approach. *SIAM J. Sci. Comput.* **31** (3), 1603–1627.
- ALI, A. & KALISCH, H. 2010 Energy balance for undular bores. *C.R. Mec.* **338** (2), 67–70.
- BAINES, P. G. 1984 A unified description of two-layer flow over topography. *J. Fluid Mech.* **146**, 127–167.
- BAINES, P. G. 1995 *Topographic effects in stratified flows*. Cambridge University Press.
- BAINES, P. G. 2016 Internal hydraulic jumps in two-layer systems. *J. Fluid Mech.* **787**, 1–15.
- BARROS, R. 2006 Conservation laws for one-dimensional shallow water models for one and two-layer flows. *Math. Models Methods Appl. Sci.* **16** (01), 119–137.
- BENJAMIN, T. B. 1968 Gravity currents and related phenomena. *J. Fluid Mech.* **31** (2), 209–248.
- BENNEY, D. J. 1973 Some properties of long nonlinear waves. *Stud. Appl. Math.* **52** (1), 45–50.
- BORDEN, Z. & MEIBURG, E. 2013 Circulation-based models for Boussinesq internal bores. *J. Fluid Mech.* **726**, R1.
- BORDEN, Z., MEIBURG, E. & CONSTANTINESCU, G. 2012 Internal bores: an improved model via a detailed analysis of the energy budget. *J. Fluid Mech.* **703**, 279–314.
- CAVANIE, A. G. 1969 Sur la genese et la propagation d'ondes internes dans un milieu a deux couches. *Cahiers Océanographiques* **XXI** (9), 831–843.
- CHOI, W. & CAMASSA, R. 1999 Fully nonlinear internal waves in a two-fluid system. *J. Fluid Mech.* **396**, 1–36.
- CHRISTIE, D. R. & WHITE, R. 1992 The morning glory of the gulf of carpentaria. *Aust. Meteorol. Mag.* **41**, 21–60.
- COURANT, R. & FRIEDRICHS, K. O. 1948 *Supersonic flow and shock waves*. Interscience, New York.
- DAVIDSON, P. A. 2001 *An Introduction to Magnetohydrodynamics*. Cambridge.
- ESLER, J. G. & PEARCE, J. D. 2011 Dispersive dam-break and lock-exchange flows in a two-layer fluid. *J. Fluid Mech.* **667**, 555–585.
- GREEN, A. E. & NAGHDI, P. M. 1976 Directed fluid sheets. *Proc. R. Soc. Lond. A* **347** (1651), 447–473.
- HÄRTEL, C., MEIBURG, E. & NECKER, F. 2000 Analysis and direct numerical simulation of the flow at a gravity-current head. part 1. flow topology and front speed for slip and no-slip boundaries. *J. Fluid Mech.* **418**, 189–212.

- HELFRICH, K. R. & MELVILLE, W. K. 2006 Long nonlinear internal waves. *Annu. Rev. Fluid Mech.* **38**, 395–425.
- HUPPERT, H. E. 2006 Gravity currents: a personal perspective. *J. Fluid Mech.* **554**, 299–322.
- HUPPERT, H. E. & SIMPSON, J. E. 1980 The slumping of gravity currents. *J. Fluid Mech.* **99** (4), 785–799.
- KALISCH, H., MITROVIC, D. & TEYEKIPITI, V. 2017 Delta shock waves in shallow water flow. *Phys. Lett. A* **381** (13), 1138–1144.
- KELLEY, D. H. & WEIER, T. 2018 Fluid mechanics of liquid metal batteries. *Appl. Mech. Rev.* **70** (2), 020801.
- KLEMP, J. B., ROTUNNO, R. & SKAMAROCK, W. C. 1994 On the dynamics of gravity currents in a channel. *J. Fluid Mech.* **269**, 169–198.
- KLEMP, J. B., ROTUNNO, R. & SKAMAROCK, W. C. 1997 On the propagation of internal bores. *J. Fluid Mech.* **331**, 81–106.
- LI, M. & CUMMINS, P. F. 1998 A note on hydraulic theory of internal bores. *Dyn Atmos Oceans* **28** (1), 1–7.
- LISKA, R., MARGOLIN, L. & WENDROFF, B. 1995 Nonhydrostatic two-layer models of incompressible flow. *Computers Math. Applic.* **29** (9), 25–37.
- LONG, R. R. 1956 Long waves in a two-fluid system. *J. Meteor.* **13** (1), 70–74.
- MARINO, B. M., THOMAS, L. P. & LINDEN, P. F. 2005 The front condition for gravity currents. *J. Fluid Mech.* **536**, 49–78.
- MILEWSKI, P., TABAK, E., TURNER, C., ROSALES, R. & MENZAQUE, F. 2004 Nonlinear stability of two-layer flows. *Comm. Math. Sci.* **2** (3), 427–442.
- MILEWSKI, P. A. & TABAK, E. G. 2015 Conservation law modelling of entrainment in layered hydrostatic flows. *J. Fluid Mech.* **772**, 272–294.
- MIURA, R. M. 1974 Conservation laws for the fully nonlinear long wave equations. *Stud. Appl. Math.* **53** (1), 45–56.
- MONTGOMERY, P. J. & MOODIE, T. B. 2001 On the number of conserved quantities for the two-layer shallow-water equations. *Stud. Appl. Math.* **106** (2), 229–259.
- OSTAPENKO, V. V. 1999 Complete systems of conservation laws for two-layer shallow water models. *J. Appl. Mech. Tech. Phys.* **40** (5), 796–804.
- OVSYANNIKOV, L. V. 1979 Two-layer "shallow water" model. *J. Appl. Mech. Tech. Phys.* **20** (2), 127–135.
- PEDLOSKY, J. 1979 *Geophysical fluid dynamics*. Springer.
- ROTTMAN, J. W. & SIMPSON, J. E. 1983 Gravity currents produced by instantaneous releases of a heavy fluid in a rectangular channel. *J. Fluid Mech.* **135**, 95–110.
- ROTUNNO, R., KLEMP, J. B., BRYAN, G. H. & MURAKI, D. J. 2011 Models of non-boussinesq lock-exchange flow. *J. Fluid Mech.* **675**, 1–26.
- SANDSTROM, H. & QUON, C. 1993 On time-dependent, two-layer flow over topography. i. hydrostatic approximation. *Fluid Dyn. Res.* **11** (3), 119.
- SCOTTI, A. & PINEDA, J. 2004 Observation of very large and steep internal waves of elevation near the massachusetts coast. *Geophys. Res. Lett.* **31** (22).
- STOKER, J. J. 1958 *Water waves: The mathematical theory with applications*. Wiley.
- UNGARISH, M. 2011 Two-layer shallow-water dam-break solutions for non-boussinesq gravity currents in a wide range of fractional depth. *J. Fluid Mech.* **675**, 27–59.
- UNGARISH, M. & HOGG, A. J. 2018 Models of internal jumps and the fronts of gravity currents: unifying two-layer theories and deriving new results. *J. Fluid Mech.* **846**, 654–685.
- WHITHAM, G. B. 1974 *Linear and Nonlinear Waves*. Wiley.
- WOLFRAM, S. 2003 *The Mathematica Book*. Wolfram Media.
- WOOD, I. R. F. & SIMPSON, J. E. 1984 Jumps in layered miscible fluids. *J. Fluid Mech.* **140**, 329–342.
- YIH, C.-S. & GUHA, C. R. 1955 Hydraulic jump in a fluid system of two layers. *Tellus* **7** (3), 358–366.